

A Recent Lindblad Resonance in the Solar Neighbourhood

J. A. Sellwood^{1*}

¹*Rutgers University, Department of Physics & Astronomy, 136 Frelinghuysen Road, Piscataway, NJ 08854-8019, USA*

8 November 2021

ABSTRACT

Stars in the solar neighbourhood do not have a smooth distribution of velocities. Instead, the distribution of velocity components in the Galactic plane manifests a great deal of kinematic substructure. Here I present an analysis in action-angle variables of the Geneva-Copenhagen survey of $\sim 14\,000$ nearby F & G dwarfs with distances and full space motions. I show that stars in the so-called “Hyades stream” have both angle and action variables characteristic of their having been scattered at an inner Lindblad resonance of a rotating disturbance potential. This discovery seems to favour spiral patterns as recurrent, short-lived instabilities.

Key words: galaxies: evolution – galaxies: kinematics and dynamics – galaxies: spiral

1 THE LOCAL DISTRIBUTION OF STELLAR VELOCITIES

The HIPPARCOS satellite (ESA 1997) obtained accurate distances and proper motions for $\sim 110\,000$ stars, but did not determine radial velocities for any. Dehnen & Binney (1998) tried to construct an unbiased sub-sample for their analyses of local stellar kinematics, and estimated the missing radial velocities statistically Dehnen (1998).

The Geneva-Copenhagen survey of nearby stars (hereafter GCS, Nordström *et al.* 2004) was designed to supply the missing velocity component for a homogeneous sample of 16 682 nearby F & G dwarf stars. This gargantuan effort has resulted in a large sample of stars in the solar neighbourhood with distances and full space motions, the latest revision of which (Holmberg *et al.* 2009) forms the basis of this paper.

The greater part of the GCS sample (14 139 stars) have multiple measurements of radial velocities to check for contamination by binaries. Holmberg *et al.* (2009) used the improved distances from the reanalysis of HIPPARCOS data by van Leeuwen (2007), but substituted photometric distance estimates for those stars with trigonometric uncertainties $> 13\%$. Proper motions are from HIPPARCOS and Tycho-2 (Høg *et al.* 2000). I do not use the disputed age estimates (*e.g.* Reid *et al.* 2007; Holmberg *et al.* 2007) in the present paper.

This monumental survey is uniquely valuable, since it is free from most of the selection biases that went into the full HIPPARCOS sample. Aside from a concentration of 112 stars in the Hyades cluster, their distribution over the sky is remarkably uniform, with a slightly higher density in the declination range south of $\delta = -26^\circ$.

The machine readable table produced by Holmberg *et al.* (2009) includes the star positions and the $U, V, & W$ components of the star’s motion relative to the Sun in Galactic coordinates.¹ Of the 16 682 stars in the table, 596 have no distance and 2536 have blank fields for the $U, V & W$ velocities. I also discard the 363 stars having distances > 200 pc from the Sun and the 112 Hyades cluster stars leaving 13 045 stars that I use in this analysis.

The median distance of these selected stars is 74 pc and the sample within 40 pc of the Sun is believed to be near complete. Nordström *et al.* (2004) do not supply individual uncertainties for each velocity, but assert that they are believed accurate to 1.5 km s^{-1} , with the greatest contribution coming from distance uncertainties. I find some evidence to corroborate this claim in the analysis presented here.

While the 112 Hyades cluster stars may seem too few in number to affect this analysis materially, I have omitted them because they are, in fact, resonant stars and would give a spurious boost to the significance of the main result (see §5.2).

Famaey *et al.* (2005) present a further sample of northern K and M giants with distances and full space motions, but rather few are close enough to have acceptably small velocity uncertainties. I have therefore not included their sample of giants in this analysis.

1.1 Phase-space Distribution

Fig. 1 confirms the salient features of Dehnen’s (1998) results, which were based on stars lacking the radial veloc-

¹ These Cartesian velocity components are oriented such that U is towards the Galactic centre, V is in the direction of Galactic rotation, and W is towards the north Galactic pole.

* E-mail: sellwood@physics.rutgers.edu

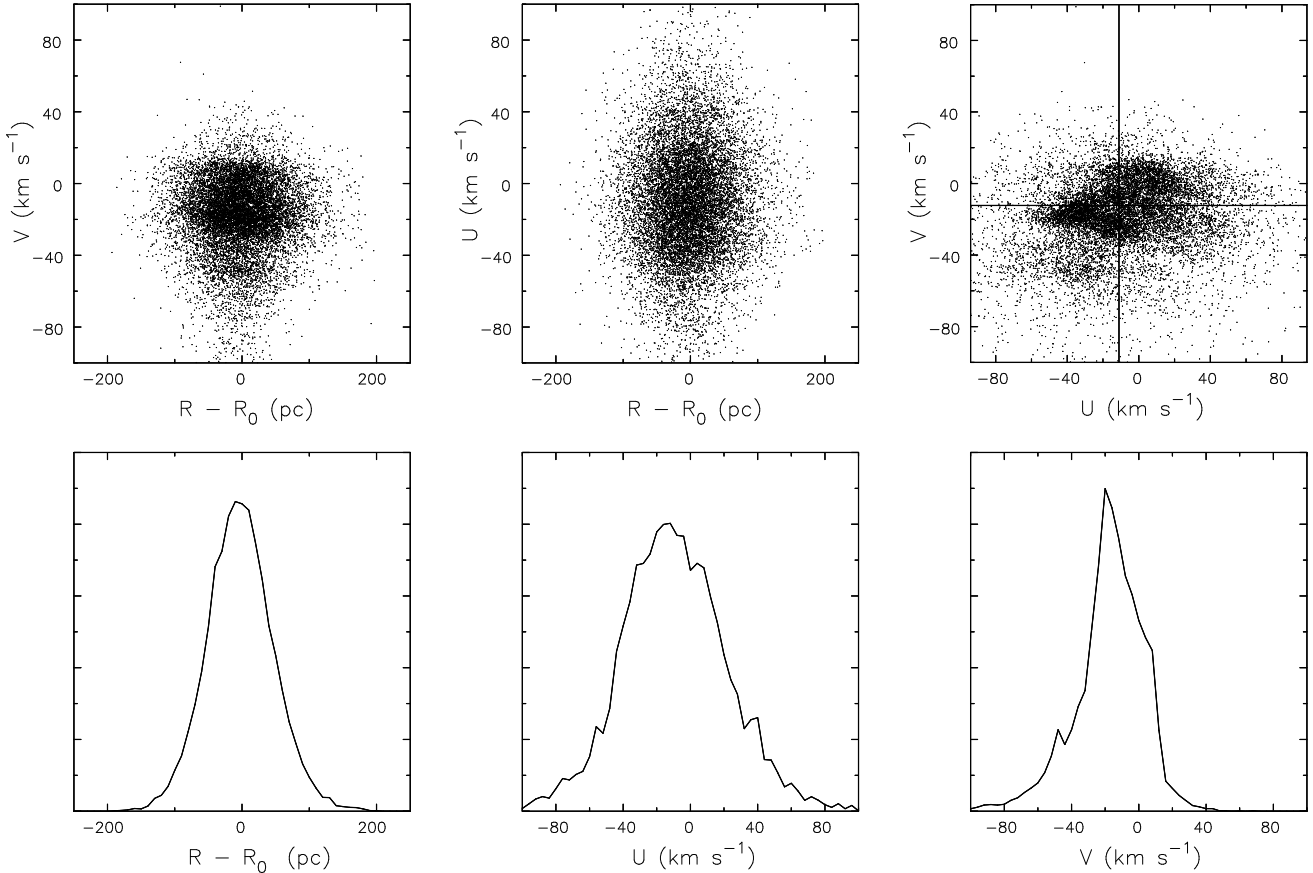


Figure 1. The lower panels show the distributions of Galacto-centric distance $R - R_0$, and the velocity components U (towards the Galactic centre) and V (in the direction of Galactic rotation) for all Geneva-Copenhagen sample stars within 200 pc of the Sun. The upper panels show three projections of the 3-D distribution; while there are no obvious correlations of either velocity component with Galacto-centric distance, the distribution in velocity space (top right) is highly non-uniform (Dehnen 1998; Nordström *et al.* 2004). The lines in the top right panel mark the LSR estimated by Schönrich *et al.* (2010).

ity, and which had residual concerns over selection biases. The “startling” aspect (Bovy *et al.* 2009) is the amount of substructure in the (U, V) plane: the distribution function (DF) of nearby stars appears to be far from simple. There is little in the way of an underlying smooth component and the entire stellar distribution is broken into several streams (Bovy *et al.* 2009). The principal streams that enter into the discussion below are labelled in Fig. 2.

The features are too substantial to have simply arisen from groups of stars that were born with similar kinematics (*e.g.* Eggen 1996), as confirmed in detailed studies (Famaey *et al.* 2007; Bensby *et al.* 2007; Bovy & Hogg 2009). It is clear that the entire DF has been sculptured by dynamical processes. While Helmi *et al.* (2006) suggest that some of the structure could be the relics of satellite accretion, most work has focused on the effects of the bar and spiral arms.

Kalnajs (1991) had previously suggested from entirely different data, that the OLR of the bar in the Milky Way might be close to the solar circle. After the release of data from HIPPARCOS, Dehnen (2000) also attributed the Hercules stream (feature C) to the OLR of the bar. De Simone *et al.* (2004), on the other hand reproduce distributions of stars with a similar degree of substructure by invoking a succession of short-lived spiral transients. Other

models that include both bars and spirals are presented by Quillen (2003), Chakrabarty (2007) and Antoja *et al.* (2009).

Quillen & Minchev (2005) associate the Hyades stream feature with 4-fold symmetric orbits in the potential of a long-lived 2-arm spiral. Such orbits arise near the ultra-harmonic (4:1) resonance of a finite amplitude perturbation, where stars make four radial oscillations in a single turn about the galaxy in a frame that rotates with the potential.

In all these studies, the spiral waves are put in “by hand”, as externally applied perturbations with properties of their choosing. The supposed spiral waves should, of course, have arisen from the stars themselves as self-consistent collective disturbances, and therefore the properties of the waves assumed by these authors may not be completely realistic. In particular, their assumed shapes and time-dependence may bias crucial resonant interactions with the stars, which are responsible for the substructure they seek to explain.

2 DISTRIBUTION IN ACTION SPACE

However, the distribution in velocity space, which these various authors attempt to mimic, is not the best projection

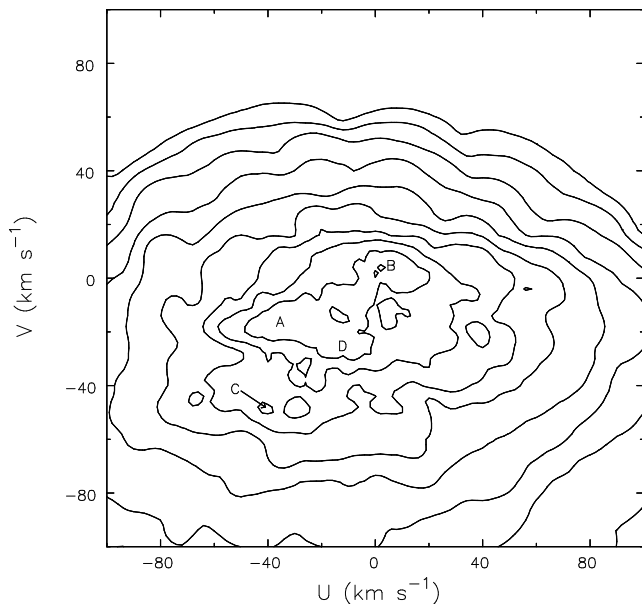


Figure 2. Logarithmically spaced contours of the surface density of stars projected in the $U - V$ -plane, as shown in Fig. 1. The letters indicate the approximate locations of the principal “star streams”: A – Hyades, B – Sirius, C – Hercules, and D – Pleiades.

of phase space to reveal the origin of the structure. A DF that is in equilibrium can be a function of the integrals only (Jeans theorem). The classical integrals for the in-plane motion in an axisymmetric disc are E & L_z , but actions (*e.g.* Binney & Tremaine 2008, hereafter BT08) are an alternative set of integrals that have a number of advantages.

In a fully phase-mixed DF, stars of a given set of actions are uniformly distributed in the conjugate angle variables in a manner that could produce a complicated structure when observed just in velocity space. Even if the DF is not completely phase mixed, so that Jeans theorem does not apply, its structure in action space is unaffected by phase mixing, and therefore should be easier to understand. Furthermore, resonant interactions with the spirals, or with the bar, are best viewed in integral space, since the only lasting changes are to the integrals (Lynden-Bell & Kalnajs 1972). In this work, therefore, I estimate action and angle variables from the observed coordinates and spatial motions of the GCS stars, and examine the stellar distribution in the space of these variables.

For motion in a spherical potential, or the symmetry plane of an axisymmetric potential $\Phi(R, z)$, the radial and azimuthal actions are (BT08, p221)

$$J_R = \frac{1}{2\pi} \oint \dot{R} dr, \quad \text{and} \quad J_\phi \equiv L_z. \quad (1)$$

Here \dot{R} is the radial speed of the star, the integral is taken around a full radial period, and L_z is the specific angular momentum of the star about the Galactic centre.

The angles, w_R & w_ϕ , conjugate to these actions both increase at uniform rates defined by $\dot{w}_R \equiv \Omega_R \equiv 2\pi/T_R$ and $\dot{w}_\phi \equiv \Omega_\phi \equiv 2\pi/T_\phi$, where the radial and azimuthal periods of the orbit are respectively defined in equations (3.17) & (3.19) of BT08. Note in the limit of nearly circular orbits, we have $\Omega_\phi \rightarrow \Omega_c$, $\Omega_R \rightarrow \kappa$, and $J_R \rightarrow \frac{1}{2}\kappa a^2$, where Ω_c ,

κ , and a are respectively the angular frequency of circular motion, the epicycle frequency, and the radius of the star’s epicycle.

I will here assume that the vertical motion of the disk stars is decoupled from their in-plane motion, or equivalently that the vertical action, J_z , is adiabatically invariant. This is justified because the vertical oscillation frequency, ν , of stars that do not climb to great heights above the disk plane is rapid compared with the motion of the star in the plane. This assumption also requires that there are no resonances between the vertical motion and rotating non-axisymmetric structures. For disk stars whose departures from circular motion are not too large, the variation in the vertical frequency around the star’s orbit can be neglected, and the vertical action may be approximated as

$$J_z = \frac{E_z}{\nu}, \quad \text{where} \quad E_z \simeq \frac{1}{2}(z^2\nu^2 + v_z^2). \quad (2)$$

The approximate form for E_z (BT08, eq. 3.86) holds for stars that do not climb to great heights above the mid-plane. Roughly two thirds of the sample remain within 200 pc of the mid-plane, while just 5% can reach z -heights $\gtrsim 500$ pc.

Aside from a well-known tendency for older stars to have larger J_z (or E_z), I have not found the distribution of J_z values revealing, and most distributions discussed in this paper are integrated over all J_z . I mention the effect of eliminating stars with large J_z in §4.3.

2.1 Evaluation of Action-Angle Variables

Evaluation of the in-plane action and angle variables for the GCS stars is impossible without knowledge of the mid-plane potential, $\Phi(R, 0)$, which is poorly known for the Milky Way. Since the rotation curve for the Galaxy in the neighbourhood of the Sun may not be far from flat locally, I adopt the mid-plane potential

$$\Phi(R, 0) = V_0^2 \ln\left(\frac{R}{R_0}\right), \quad (3)$$

with the R_0 being the radius of the solar circle, and V_0 being the orbital speed of the local standard of rest (LSR). I correct for solar motion by adding the peculiar velocity of the Sun (11.1, 12.24, 7.25) km s^{-1} (Schönrich *et al.* 2010) to the tabulated (U, V, W) components. I note below (§4) that the results in this paper are insensitive to this choice.

In order to compute the four action-angle variables, $(J_R, J_\phi, w_R, w_\phi)$, I integrate the orbit of every star in the GCS sample in this potential from its observed position. I normalize both actions by dividing them by the specific angular momentum of the LSR, $L_{z,0} = R_0 V_0$; my adopted values of these constants ($R_0 = 8$ kpc and $V_0 = 220$ km s^{-1}) determine only the scaling of the actions and other choices would not alter the conclusions. I choose $w_R = 0$ at the apocentre of a star’s epicycle and $w_\phi = 0$ at the azimuthal location of the Sun.

This procedure implies two major assumptions. First, the Milky Way rotation curve is locally flat; adjustment for a different potential would merely distort the distribution of stars in the space of these variables as points on a stretched rubber sheet. Second, I have assumed an axisymmetric potential, whereas the Milky Way certainly has at least mild non-axisymmetry: the large majority of stars in the GCS

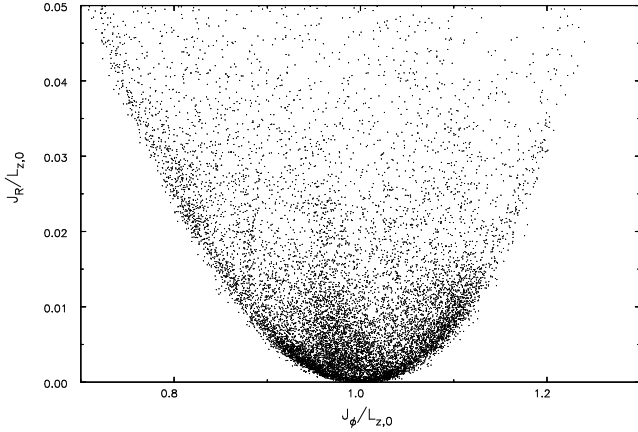


Figure 3. The distribution of GCS stars in the space of the two actions $J_R/L_{z,0}$ and $J_\phi/L_{z,0}$. The approximately parabolic lower boundary reflects the selection of stars from the solar vicinity. Aside from the general decrease in density towards large J_R and a skew to lower J_ϕ caused largely by the asymmetric drift, the DF in this projection also shows significant substructure.

sample have orbits that do not take them more than ~ 2 kpc from the orbit of the Sun, and most stay much closer. This range of distances is large enough for them to experience some non-axisymmetric changes in the gravitational potential. The instantaneous values of these integrals at the solar azimuth must differ in a periodic manner from those for similar stars at other azimuths, but the ordering of stars in J_ϕ and J_R should not be affected, since the LSR also follows the same non-axisymmetric potential. Thus, neither assumption affects the topology of the distribution of stars in these variables, and no features in the distribution could be erased or appear if they were corrected. Therefore, neither these assumptions, nor uncertainties in the Galactic constants, R_0 & V_0 , compromises the principal scientific finding of this paper.

2.2 Results

Fig. 3 shows the distribution of GCS stars in action space, excluding the small fraction (994 stars) with $J_R/L_{z,0} > 0.05$ (*i.e.* with epicycle radii $a \gtrsim 2$ kpc). The near-parabolic lower boundary of the distribution reflects the fact that all the stars in this sample are currently within 200 pc of the Sun, and therefore must have ever more eccentric orbits (larger J_R) as their guiding centre radii, or J_ϕ , differ increasingly from that of the Sun.

The general decrease in density with increasing J_R is expected in any reasonable stellar distribution, and the asymmetry between left and right results from the fact that the star density increases towards the Galactic centre; more stars visit the solar neighbourhood from the interior, which gives rise to the asymmetric drift. It is clear from this Figure that the distribution in the space of these integrals also has substructure; the most notable feature is a pronounced overdensity of stars rising with slightly negative slope from $J_\phi \lesssim L_{z,0}$.

Fig. 4 shows the distributions of angle variables for the same stars. We should expect fewer stars in the upper panel near $w_R = \pm\pi$ and near $w_R = 0$, because such stars are

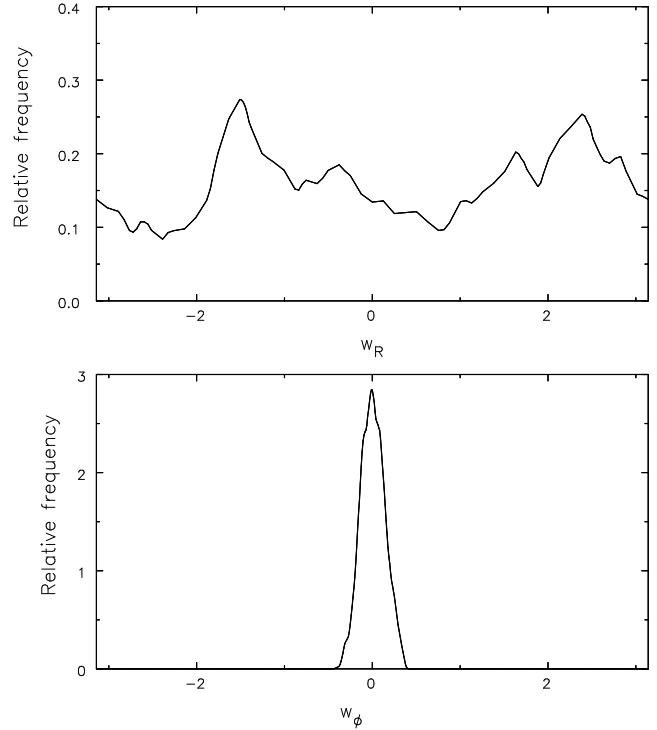


Figure 4. The upper panel shows the distribution of angular phases, w_R , while the lower panel shows the distribution of azimuthal phases, w_ϕ , for the GCS stars.

visiting the solar neighbourhood at respectively the peri- and apo-centres of their orbits. The fact that the peaks are not symmetrically placed near $w_R = \pm\pi/2$ is interesting, as discussed below. The azimuthal phase distribution has a single strong peak near $w_\phi = 0$ because the stars are all local to the solar neighbourhood. The width of this peak, which has a half-width at half-maximum of $\sim \pm 11^\circ$, reflects the spread in Galactic azimuths of the guiding centres for stars currently passing by the Sun.

3 EXCHANGES AT RESONANCES

The upper panel of Fig. 5 shows the Lindblad diagram for a Mestel disk with an infinitesimal perturbation of constant pattern speed $\Omega_p = 0.14$, chosen arbitrarily. The full-drawn curve marks the locus of circular orbits in this (L_z, E) plane; no star can lie below this curve, but bound stars with $E > E_{\text{circ}}$ move on eccentric orbits in this potential.

When the potential includes an m -fold rotational symmetric perturbation with pattern speed Ω_p , stars orbiting in the disc encounter wave crests at the Doppler-shifted frequency $m|\Omega_p - \Omega_\phi|$. Resonances arise when

$$m(\Omega_p - \Omega_\phi) = l\Omega_R, \quad (4)$$

with $l = 0$ at corotation, and $l = \pm 1$ at the Lindblad resonances where the guiding center respectively overtakes, or is overtaken by, the wave at the star's unforced radial frequency.² The loci of these three principal resonances for arbitrarily eccentric orbits are marked by the broken curves in

² Note $|l| = 1/2$ at ultraharmonic resonances.

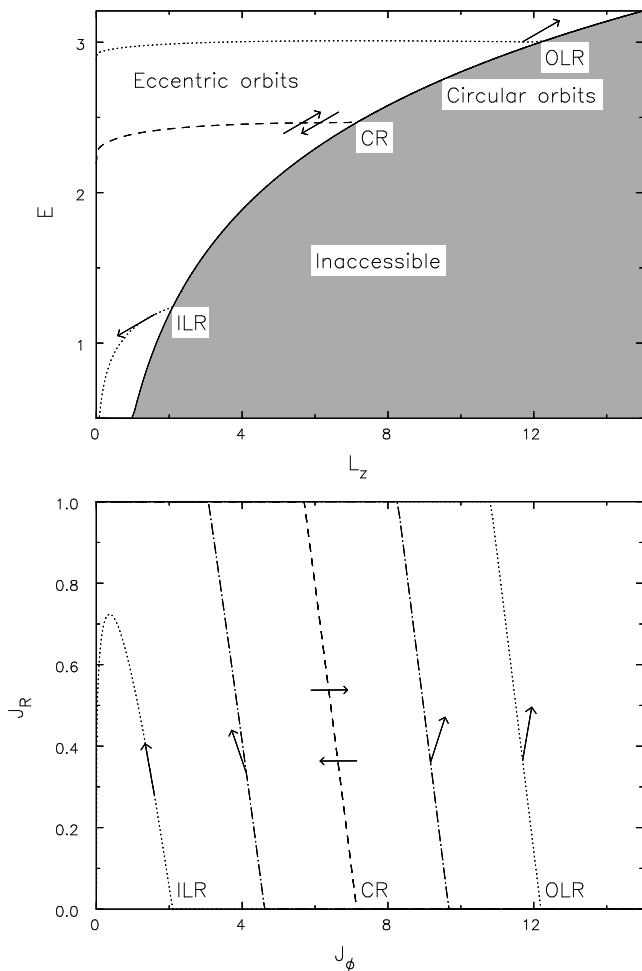


Figure 5. The upper panel shows the Lindblad diagram for a simple disk galaxy model. Circular orbits lie along the full-drawn curve and eccentric orbits fill the region above it. Angular momentum and energy exchanges between a wave and stars move them along lines of slope Ω_p as shown. The dotted and dashed lines show the loci of resonances for an $m = 2$ perturbation of arbitrary pattern speed. The lower panel plots the same resonance lines and scattering vectors in action space, where $J_\phi = L_z$ and circular orbits lie on the axis $J_R = 0$. The dot-dashed lines in the lower panel show the Lindblad resonances for an $m = 4$ disturbance having the same pattern speed.

this Figure, which intersect the circular orbit curve where the more familiar epicyclic definitions of resonances apply. These lines are drawn for a bi-symmetric ($m = 2$) disturbance; the Lindblad resonances would be closer to corotation for $m > 2$.

Stars moving in a non-axisymmetric potential that rotates at a steady rate conserve neither their specific energy, E , nor their specific angular momentum, L_z . But the combination

$$I_J \equiv E - \Omega_p L_z, \quad (5)$$

known as Jacobi’s invariant (BT08, eq. 3.112), is conserved. Therefore, when a star changes its angular momentum by an amount ΔL_z caused by the rotating potential disturbance, it also changes its energy by the amount

$$\Delta E = \Omega_p \Delta L_z. \quad (6)$$

Thus changes to these classical integrals caused by interactions with a steadily rotating disturbance have slope Ω_p in the Lindblad diagram.

Lynden-Bell & Kalnajs (1972) showed that a lasting change to the angular momentum of a star can occur only at resonances. As the slope of the circular orbit curve at corotation is Ω_p , stars that exchange energy and angular momentum there do not move away from that curve, to first order, enabling exchanges to occur without heating, as described by Sellwood & Binney (2002). The other vectors show that exchanges at the Lindblad resonances, on the other hand, cause stars to move onto more eccentric orbits (farther from the circular orbit curve) when angular momentum is redistributed outwards. This is the root cause of disk heating by spirals.

The lower panel of Fig. 5 shows in action space the same resonance lines and scattering vectors as the upper panel shows for the space of the classical integrals. Exchanges at corotation cause horizontal shifts, implying no increase in J_R , while gains in J_ϕ at the outer Lindblad resonance, hereafter OLR, and losses at the inner Lindblad resonance (ILR) both cause increases in J_R . The labelled resonance lines are drawn for $m = 2$ and an arbitrarily chosen value of Ω_p ; the diagram for other adopted pattern speeds in this scale-free potential would have a similar appearance, but with the J_ϕ -axis rescaled. The dot-dash lines in the lower panel mark the Lindblad resonances for an $m = 4$ wave of the same pattern speed, with the scattering vectors again shown.

Notice that the direction of the scattering vector closely follows the resonant locus for $m = 2$ (dotted curve) only at the ILR. Thus, when stars are scattered at this resonance, they stay on resonance as they gain random energy, allowing very strong scatterings to occur. The opposite case arises at the OLR, where the star is moved off resonance by a small gain of angular momentum. The alignment is closest for $m = 2$ disturbances in potentials that yield flat rotation curves, but scattering is always stronger at the ILR than at the OLR for $m \geq 2$ and in more general potentials.

All three resonance lines have similar, though not identical, slopes in the action plot and for all $m \geq 2$. Thus resonant stars will lie along a line in action space that has approximately the same negative slope for any resonance. However, we can identify the resonance at which they were scattered or trapped by examining the angles, since the resonance will have reset the values of the phase angles for trapped stars to have the relation

$$mw_\phi + lw_R = \text{constant}, \quad (7)$$

where l and m were defined above. Both angles increase with time but the equation continues to hold at any fixed time because resonant stars have $m\dot{w}_\phi + l\dot{w}_R = m\Omega_p$. Thus the value of the “constant” in eq. (7) varies as $m\Omega_p(t - t_0)$, but from an unknown value at some earlier t_0 that depends upon the phases of the stars relative to the perturbation. We will use eq. (7) in § 4.2.

4 IDENTIFICATION OF RESONANCES

While the principal feature in Fig. 3 is clear to the eye, I need a method to determine its statistical significance and

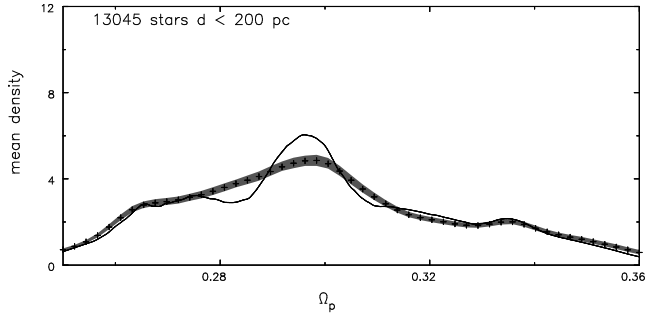


Figure 6. The solid line shows mean density of GCS stars in the (J_ϕ, J_R) plane along scattering trajectories from circular orbits, as a function of the pattern speed of the perturbation. The shaded region shows the 99% confidence limits from similar size star samples with randomly selected Galacto-centric distance and velocity components.

to search for possible weaker features. This requires a statistic that contrasts the data with a comparable featureless model. Ideally, a suitable featureless model would have a simple distribution function but the velocity distributions shown in Fig. 1 are not simple; the U -distribution is not Gaussian (it has a large kurtosis), while the V -distribution is complex and skew. Thus no simple function of the integrals could yield a DF that would be an approximate match to the density of GCS stars in action space.

4.1 Statistical Significance

I therefore adopt a bootstrap approach in which I resample the actual distributions of R , U & V to generate comparison distributions of pseudo stars. Selecting all three coordinates independently destroys the correlations that give rise to any features in integral space. While such a procedure could be dangerous if the velocity components have large and widely differing errors, the velocity and distance errors in the present sample are all small with respect to the ranges of the data. Samples of pseudo data selected in this way populate the (J_ϕ, J_R) -plane in a very similar manner to the real data, but with any small-scale structure smoothed away.

As a quantitative estimator of structure, I compute the mean surface density of stars in (J_ϕ, J_R) space along resonance lines. I estimate the surface density of stars in the (J_ϕ, J_R) -plane using an adaptive smoothing kernel (Silverman 1986) of elliptical shape with axis ratio 12:1 to compensate for the differing ranges of J_ϕ and J_R . To compute the mean density as a function of Ω_p , I integrate the estimated star density in this plane along a resonance line for that selected Ω_p . The path of integration is from where the resonance line intersects the lower boundary of the stars to $J_R = 0.05$; dividing by the length of this line yields the mean density.

Figure 6 compares the mean density along ILR lines for a range of Ω_p with 99% confidence intervals (shaded) of the same quantity selected from 2000 samples of scrambled data. The Figure indicates one highly significant feature with a pattern speed $\Omega_p \sim 0.296 \pm 0.005$. No other feature is nearly as significant. Repeating this analysis for trapping at corotation and at the OLR, again revealed a single feature of high significance.

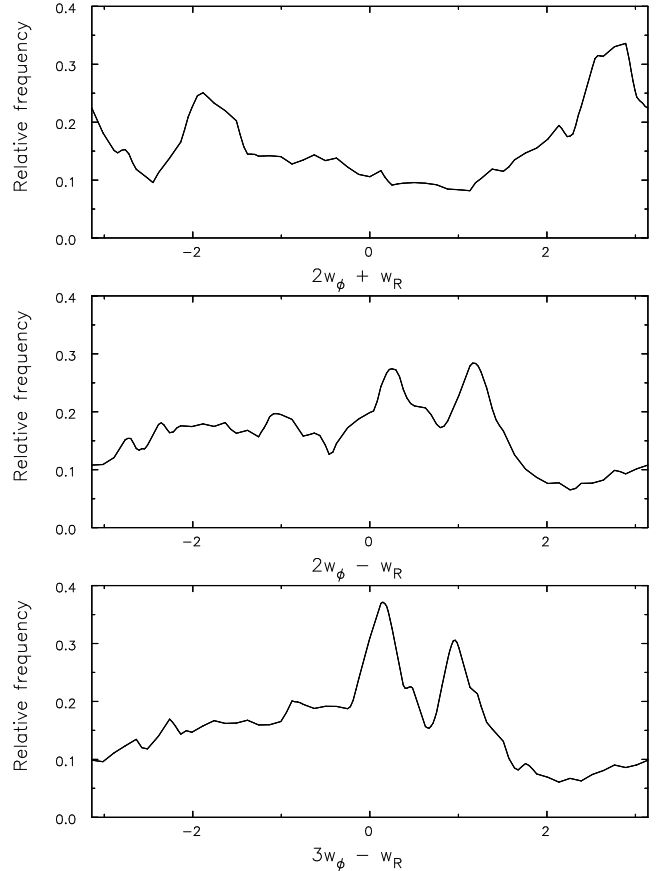


Figure 7. The distribution of three linear combinations of phase angles as tests for correlations characteristic of resonances.

In §4.3, I report the results of tests for possible selection biases in this sample of stars that might affect the significance of the feature detected in Figure 6.

Figure 6 assumed a bisymmetric spiral pattern, but it is possible the resonance arose from a spiral having higher rotational symmetry. Repeating the analysis assuming $m = 3$ & 4 revealed maxima that were no less significant from that for $m = 2$ but having different frequencies. Thus not only do the action data not determine which resonance is responsible, but they do not determine the rotational symmetry of the pattern either.

4.2 Phases

We can tell which resonance was responsible for the density excess in the (J_ϕ, J_R) -plane by examining the distribution of phase angle variables for the stars. The distribution of w_R (Fig. 4) has two peaks away from zero radians, while the distribution of w_ϕ values is narrow because all the stars in the sample are near the Sun. Because of this selection effect, we should expect the distribution of combinations of $mw_\phi \pm w_R$ to resemble that of $\pm w_R$ alone, were the two angle variables uncorrelated.

Fig. 7 shows the distributions, modulo 2π , of three linear combinations of the two angle variables. Our expectation is borne out in the top panel, but not in the two lower panels. The change in shape of the distribution is quite dramatic, indicating significant correlations that are characteristic of

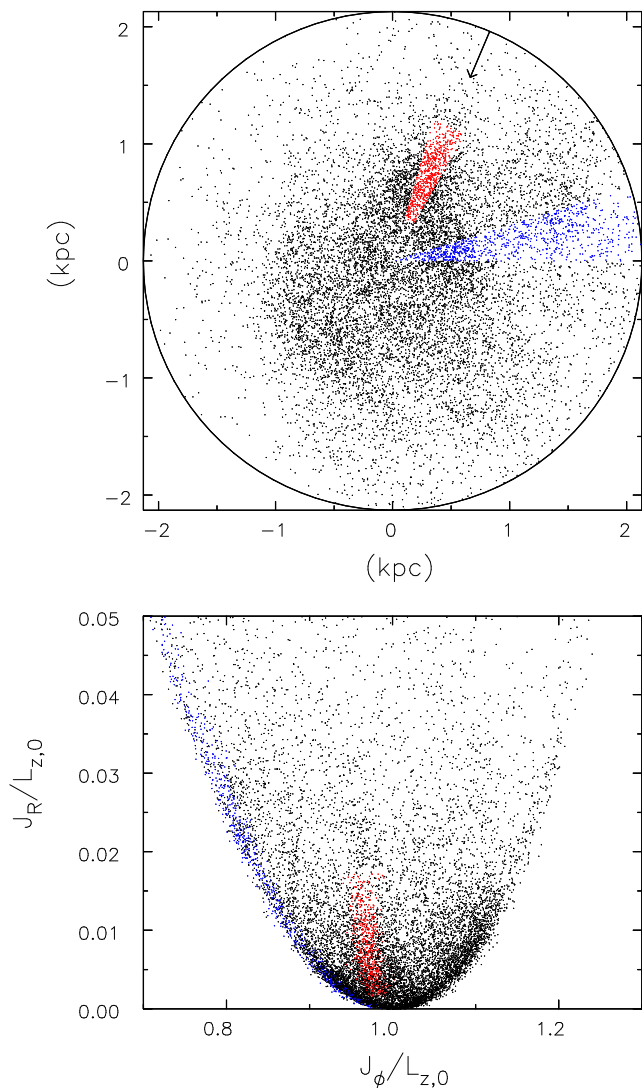


Figure 8. The upper panel shows the distribution of GCS stars in the space of the epicycle amplitude and spiral phase. The radial coordinate is $a = (2J_R/\kappa)^{1/2}$, and the azimuthal coordinate is $2w_\phi - w_R$. The lower panel is the same as shown in Fig. 3, except it uses the colours assigned in the upper panel.

an ILR for a pattern. The lower two panels assume patterns having two- or three-fold rotational symmetry ($m = 2$ or 3). The peak near zero, which becomes more significant as m is increased, is a selection effect, while the feature of most interest is the second peak away from zero, which is still present for $m = 4$ (not shown). It is made up of stars having negative w_R values near the peak shown in Fig. 4 that also have slightly negative values of w_ϕ .

To investigate further, the upper panel of Fig. 8 shows the distribution of the GCS stars in polar coordinates of the epicycle radius $a = (2J_R/\kappa)^{1/2}$ and polar angle $2w_\phi - w_R$ as appropriate for stars trapped at an ILR of an $m = 2$ pattern. The two peaks in the middle panel of Fig. 7 indicate concentrations of stars near $2w_\phi - w_R \sim 0.15$ and 1.17 , or 9° and 67° . I have coloured the stars in these concentrations; all those having $2w_\phi - w_R = 67^\circ \pm 7^\circ$ and moderate radial action are coloured red, while those in the range $2w_\phi - w_R = 9^\circ \pm 9^\circ$ are coloured blue.

I have then used this colouring to show, in the lower panel, the locations of the same stars in the plot of actions, reproduced from Fig. 3. The blue stars are concentrated along the boundary of the lower plot, indicating that they are all close to the apocentres of their orbits and the concentration at this phase, discussed below, is probably of little dynamical significance. However, the red stars coincide with the resonance peak identified earlier.

The boundaries of the triangle in the upper panel of Fig. 8 enclose 639 stars. These geometrically simple boundaries are not intended to select all or only resonant stars, but it is likely that most of the selected stars are resonant. It is also likely that additional resonant stars lie outside these somewhat arbitrary boundaries.

If we assume a m -arm spiral, we should change the polar angle to $mw_\phi - w_R$. Polar plots for the cases $m = 3$ & 4 (not shown) are very similar to the upper panel of Fig. 8 except that the “red” stars are now concentrated at smaller angles, with almost equal significance. Furthermore, almost the *same set* of stars form the local peak of the distribution of $mw_\phi - w_R$ for $m = 3$ & 4 as for $m = 2$, and they therefore again lie in the density excess in the action plot (lower panel).

It is the correspondence between the stars of the selected phases that also have values of their actions to place them in the scattering peak that provides the most compelling evidence for an ILR. But once again the evidence cannot discriminate whether the stars were trapped by an $m = 2$ wave, or one having higher rotational symmetry.

4.3 Further Tests

I have conducted an extensive series of tests to check the result in Fig. 6. The main concern is that the apparently resonant stars stand out because they share some other property unrelated to a resonance.

Some 37% of the GCS stars are known or suspected binaries. The significance of the resonance peak is unaffected by including or eliminating the stars flagged as possible or known binaries.

Increasing the kernel width used to estimate the density in the (J_ϕ, J_R) -plane (default = 0.02) smoothed the curve in Fig. 6 and lowered the maximum as expected. But it also reduced the ranges of the confidence intervals, so the feature remained highly significant.

The principal source of uncertainty in the input data arises from the uncertainty in the distance to each star, which generally rises with distance to the star. I therefore repeated the analysis using stars lying within various distances from the Sun ($d < 50$ pc at the most extreme), which had little effect on either the significance or the position of the principal peak in the upper panel of Fig. 6.

Performing the same analysis on stars separated into opposite hemispheres on the sky, either in equatorial or Galactic coordinates, did not affect the significance of the peak. Since the spectroscopic radial velocities could be more precise than those derived from the proper motion, I tried separating the stars into samples within 60° of the Galactic poles from those lying closer to the plane. The radial velocity contributes little to the U & V velocity components for stars near the caps, but the scattering peak in this case is just as significant as for the remaining stars. I also tried sep-

Table 1. Estimated pattern speeds and corotation radii for the fitted disturbance. The possible systematic errors in these quantities are much greater than the small statistical uncertainties.

Angular periodicity	$\Omega_p R_0 / V_0$	Ω_p km s ⁻¹ kpc ⁻¹	R_{CR} kpc
$m = 2$	0.296	8.1	27
$m = 3$	0.534	14.7	15
$m = 4$	0.655	18.0	12

arate analyses for stars in quadrants centred on the Galactic centre and anti-centre, from those in quadrants centred on the apex and ant-apex of Galactic rotation, again finding little change.

Finally, I investigated the effects of dividing the sample using by the energy of vertical motion, E_z (eq. 2). The resonance peak is most significant among the stars in the lowest $\sim 66\%$ of the vertical energy range, and much less significant in the other 33%. Such a dependence seems entirely reasonable, since stars with larger vertical oscillations will be much less affected by in-plane potential variations.

These various tests have proved reassuring. The effects of selecting subsamples of the stars are all entirely consistent with physical expectations, and the likely influence of the small errors in the quantities tabulated in the catalogue.

4.4 Adjustments to the LSR

The local standard of rest (LSR), which is the speed of a particle on a notional “circular orbit” passing through the Sun’s position, may not even be well-defined because the Galaxy is at least mildly non-axisymmetric. Furthermore, the Sun’s speed relative to the LSR is hard to determine, and estimates by Binney and his collaborators (Dehnen & Binney 1998; Aumer & Binney 2009; Schönrich *et al.* 2010) from the HIPPARCOS data have changed by several km s⁻¹ at each revision.

As the values of the action-angle variables depend on the choice of the LSR, I have experimented with adopting values that differ from the latest estimate (Schönrich *et al.* 2010) by ± 10 and ± 20 km s⁻¹ in both U and V . Shifting the V -component essentially shifts the entire distribution in Fig. 3 to the left or right while preserving most of the structure. For larger revisions to the LSR, the upward rising tongue becomes rather broader, however. Furthermore, the distribution of the angle variables is not changed qualitatively, and I always obtain peaks in the distribution of $m w_\phi - w_r$ for $m = 2, 3$ & 4 that are located away from the direction towards the Galactic centre. Thus the main finding of this paper is little affected by the precise choice of the LSR.

5 DISCUSSION

Fig. 8 provides strong evidence that a small fraction ($\sim 5\%$) of the GCS stars have been trapped at an ILR of a rotating disturbance.

5.1 Angular Periodicity

It is indeed surprising to find evidence for an ILR near the Sun, as it seems to imply a spiral pattern extending outwards from the Galactic radius of the Sun’s orbit. However, none of the foregoing analysis could discriminate whether the ILR was that of a bisymmetric pattern or one of higher rotational symmetry.

Assuming $R_0 = 8$ kpc and $V_0 = 220$ km s⁻¹, and using the evidence that the scattering peak was caused by an ILR, we may determine the pattern speed of the disturbance from the frequency at which the mean density in Fig. 6 peaks. Table 1 gives, for each angular periodicity, the measured frequency of the peak, and the implied pattern speed and corotation radius, also assuming an exactly flat rotation curve. (The statistical uncertainty in the measured Ω_p is $\lesssim 2\%$, but systematic errors arising from the various assumptions are likely to be much larger.) While the Milky Way rotation curve may not be exactly flat, it is clear that corotation lies in the far outer disk for all of these patterns.

If the disturbance responsible for the ILR is a spiral pattern (it could be some other slowly rotating disturbance), one would expect corotation to lie within the disk of the Milky Way, which probably does not extend much beyond a Galacto-centric radius of 14 kpc (Robin *et al.* 1992, but see also Carraro *et al.* 2010). This argument would strongly disfavour an $m = 2$ spiral, but the Milky Way disk may be extensive enough to accommodate spirals of higher rotational symmetry.

Quillen & Minchev (2005) calculated the appearance of the (U, V) -plane in a simple galaxy model that was perturbed by a large-amplitude, long-lived, bi-symmetric spiral that rotated with various pattern speeds. For a pattern speed low enough to place the ILR near the Sun, the phase-space structure they calculated did not correspond well with that observed, but higher pattern speeds that placed the Sun near the ultraharmonic resonance of their assumed spiral created a feature resembling the Hyades stream. They showed that the orbits responsible were 4:1 resonant periodic orbits in their adopted pattern. Unlike in their work, my analysis makes no assumption about the spatial form or lifetime of the potential perturbation, but the fact that they favoured 4:1 periodic orbits as the cause of the Hyades feature may be hinting that an $m = 4$ spiral perturbation is favoured.

5.2 Properties of the Resonant Stars

The upper panel of Fig. 9 shows that the 639 stars that I coloured red in Fig. 8 lie in the “Hyades stream” in (U, V) -space (feature A of Fig. 2). Note that the highlighted stars do not include all the resonant stars; thus the fact that not all the Hyades stream stars are coloured, and that a few coloured stars are outside the stream may not be significant (see §5.4). It therefore seems clear that the larger part of the Hyades stream is caused by the ILR identified here.

Aside from their kinematics, I have been unable to find any property of these 639 stars that clearly differs from the parent distribution of the GCS sample. They have a similar distribution of distances, and incidence of binarity, for example. Note that Famaey *et al.* (2007) do find a mild, but significant, metallicity excess among the Hyades stars com-

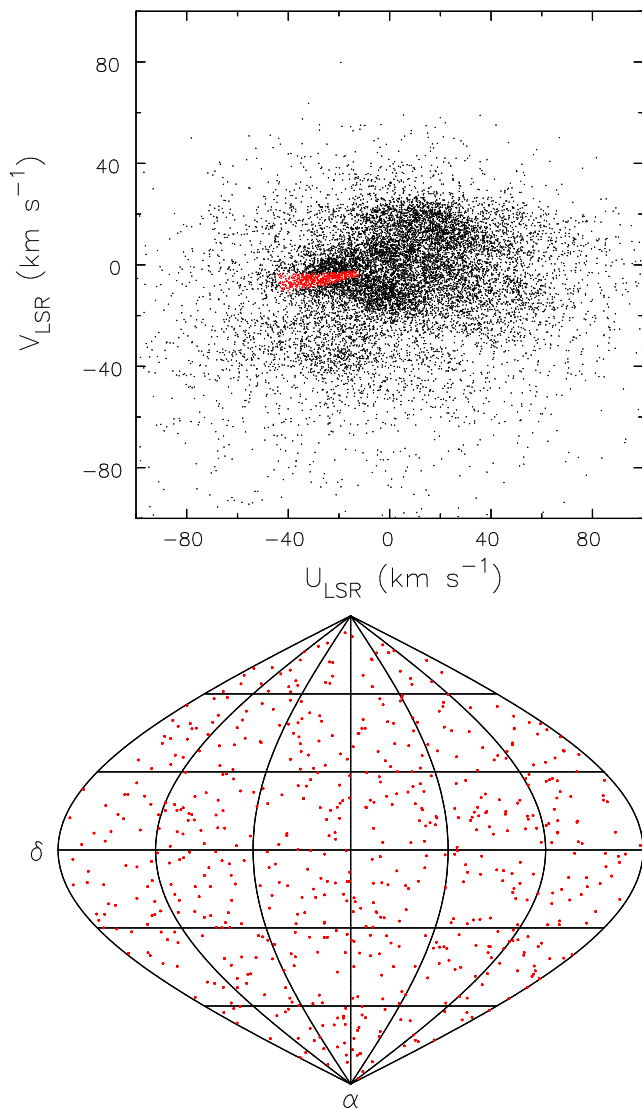


Figure 9. The upper panel reproduces the distribution of GCS stars in the top-right panel of Fig. 1, but with those shown in red being the 639 stars picked out in Fig. 8. The lower panel shows the positions, in right ascension and declination, of the highlighted stars.

pared with the mean for the GCS, although Bovy & Hogg (2009) find they are “barely distinguishable” from the background population.

The lower panel of Fig. 9 shows that the 639 red stars are almost uniformly distributed over the sky. Note that I have excluded stars in the Hyades cluster itself from all the analysis because it would be wrong to treat all the stars within a gravitational bound cluster as if they were dynamically independent. Had I included the cluster, an additional 84 of the 112 Hyades stars would have been coloured red in Fig. 8, the resonant feature would have appeared yet more significant, and the cluster would have stood out as a strong concentration near $(\alpha, \delta) = (4^{\text{h}} 27^{\text{m}}, 15^{\circ} 52')$. Thus the Hyades cluster itself is resonant.

5.3 The Age of the Resonance

Were reliable ages for the stars available, we could use them to date the origin of the scattering peak, since it can contain stars of all ages except those that are younger than the wave that caused it. This is because the gas from which stars form is not subject to the laws of collisionless dynamics; a gas cloud in a resonance will experience the same gravitational accelerations as do the stars, but dissipative collisions will quickly destroy the resonant signature in phase space.

While age estimates for individual stars appear to be unreliable (Reid *et al.* 2007; Holmberg *et al.* 2007), we can at least use the Hyades cluster, which does appear to be resonant (§5.2). The cluster must have been formed before the perturbation that scattered it, which places an upper bound on the time since the resonance of 648 ± 45 Myr (*e.g.* De Gennaro *et al.* 2009).

We can also use the spread in the spiral phase, or the width of the peak in Fig. 7, to argue that the perturbation must have been recent. Assuming spirals to be transient, the resonance will have had a width, $\Delta\Omega_p = 0.1\Omega_p$, say. Thus the width of the spiral phase will increase with time as $\Delta(mv_\phi + lw_R) = 0.1m\Omega_p(t - t_0)$. A generous estimate of the width of the peak is 0.3 radians (or $\sim 19^\circ$, over twice the width of the red triangle in Fig. 8) and therefore the time since the resonance $t - t_0 < 0.3/(0.1m\Omega_p)$, where the inequality arises because the width can only be increased by measurement error. The value of Ω_p is given by the position of the peak in Fig. 6, or $\Omega_p = 0.3V_0/R_0$. Using $R_0 = 8$ kpc and $V_0 = 220$ km s $^{-1}$ and adopting $m = 2$, I find $t - t_0 \lesssim 180$ Myr, or the resonance occurred within the last Galactic rotation. This rough calculation made a number of assumptions; assuming a sharper resonance or a broader spread of spiral phases would increase the time scale, but the values adopted seem reasonable. It is reassuring that this estimate is substantially less than the age of the Hyades. I therefore conclude that the resonance is indeed very recent.

Note that not only will phase mixing blur resonances in angle space, but we must expect resonant features to become less distinct in action space over time because stars are also scattered by giant molecular clouds (*e.g.* Binney & Lacey 1988). The rate is hard to quantify, however, since the rate of cloud scattering is uncertain (Lacey 1991; Hänninen & Flynn 2002).

5.4 Other “Streams”

Since the red stars in Fig. 8 turned out to be the Hyades stream, I have attempted to identify in the same Figure the other principal features named in Fig. 2. I have coloured all the GCS stars lying in selected elliptical areas in velocity space in the top panel of Fig. 10, and the same colours are used for each star in the lower two panels. Again I use red for the Hyades region, but here the selection deliberately errs on generous side to include most of the stream stars and more besides.

Tracing these stars in other panels reveals that most of the Hyades stream stars lie in the resonance ridge in Fig. 3 and have the range of phases that yielded the peak in Fig. 7. The Sirius stream (green) appears not to be resonant, as its stars extend over a significant range of J_ϕ but not in J_R , and

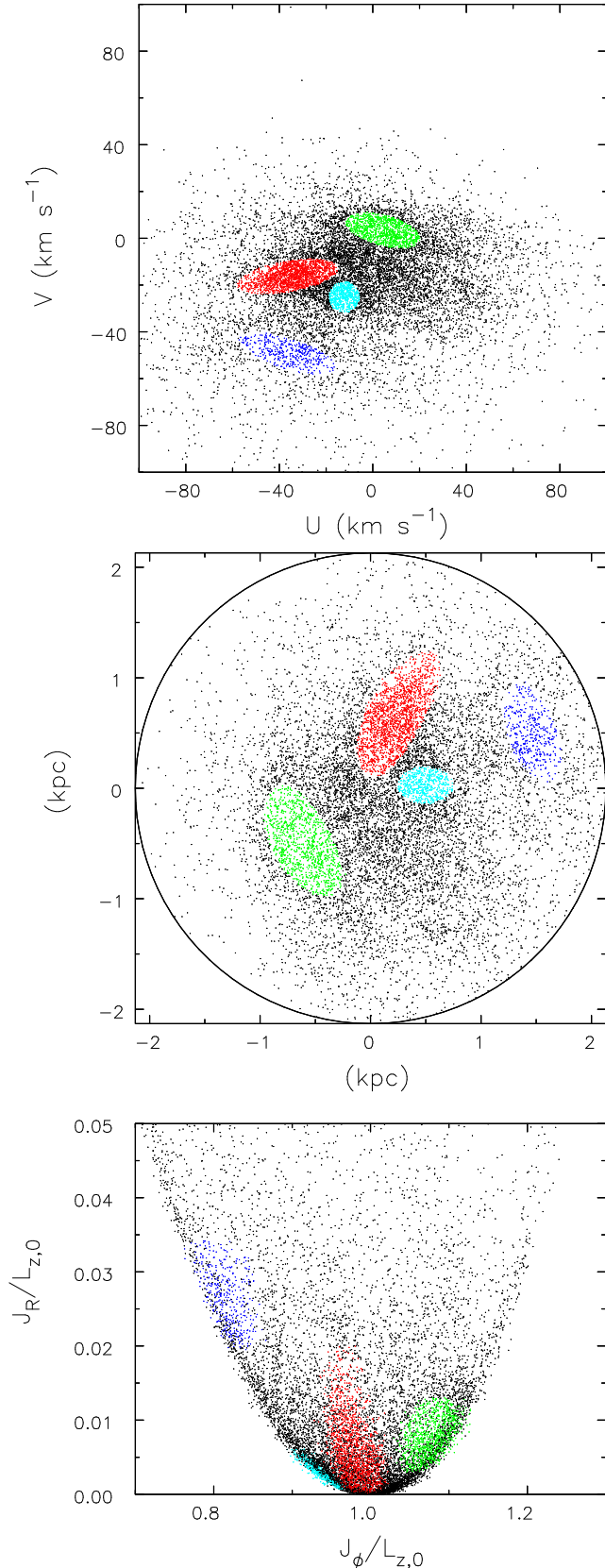


Figure 10. The top panel assigns colours to some of the stars near the centres of the different streams: Hyades – red, Sirius – green, Hercules – dark blue, and Pleiades – cyan. The same colour codes are used to show the locations of these streams in the distribution of action and angle variables in the lower two panels.

have no special concentration in phases. Both the Pleiades (cyan) and Hercules (blue) stars are near the low- J_ϕ boundary of the sample and may be parts of larger structures that extend outside the sample, if so their range of phases may be limited. This selection effect makes it impossible for this diagnostic to determine whether they are associated with a resonance.

5.5 Implications for Spiral Structure Theory

The identification of an ILR in the solar neighbourhood is a powerful discriminant between the different theories of spiral pattern generation. It has long been known that spiral waves are damped at an ILR (*e.g.* Binney & Tremaine 2008, p. 502). Bertin & Lin (1996), who argue that spiral patterns are long-lived waves, therefore require the ILR to be shielded in order to avoid fierce damping. Thus evidence for an ILR excludes their quasi-steady spiral hypothesis as the originating mechanism for the disturbance that created it. While this evidence does not exclude the possibility of steady spirals elsewhere, it seems unattractive to invoke a different mechanism to account for spirals in places other than where we can mount a test.

Strong ILR damping of individual patterns therefore requires spirals to be continuously regenerated in order that they be common features in galaxies. While Toomre & Kalnajs (1991) envisage spiral patterns as recurring transient responses, only my idea (Sellwood & Lin 1989; Sellwood 2000) invokes resonant scattering as the *cause* of a recurrent cycle of true instabilities. Indeed, I predicted (Sellwood 1994) that such a feature might be visible in the HIPPARCOS data.

6 CONCLUSIONS

The foregoing analysis and tests provide compelling evidence that the “Hyades stream” in the solar neighbourhood has been created through scattering at a recent inner Lindblad resonance. The strongest evidence is that the stars clustered over a narrow range of the combination of angles expected for an ILR are also those that lie in the highly significant overdensity in action space, as indicated by those coloured red in Fig. 8. These same stars, which are distributed all over the sky, make up the Hyades stream as shown in Fig. 9.

Bovy & Hogg (2009) construct a plot similar to Fig. 3, also using the GCS sample but restricted to the ~ 9500 stars within 100 pc of the Sun. Instead of using radial action as the ordinate, their Figure 17 uses the almost equivalent energy of non-circular motion, $E - E_c$, and they scale their plot to include a larger range of epicycle sizes. Because of the difference in scale, the feature I report here is rather inconspicuous in their Figure, but their aim was to test for the feature I had claimed a hint of in Sellwood (2000).

Thus only the Hyades stream (feature A of Fig. 2) can be attributed to this ILR and the remaining structures in the local phase space distribution must be accounted for in other ways. It is likely that the OLR of the bar in the Milky Way accounts for the Hercules stream (feature C, Dehnen 2000), but we still lack convincing models to account for the Pleiades and Sirius streams. Since neither feature stands out

in Fig. 10 (see also Fig. 17 of Bovy & Hogg 2009), these kinematic groupings of stars have probably not been caused by resonances with spirals, although they could perhaps still reflect the continued presence of spirals in this part of the disc with the resonances lying elsewhere (*e.g.* De Simone *et al.* 2004).

Most theoretical studies of spiral structure start with the assumption that the DF of disk stars is smooth and featureless. The immediate implication of a prominent feature in Fig. 3 is that this assumption is incorrect. The fact that it was created by an ILR is strong evidence against the disturbance being a quasi-steady spiral of the kind proposed by Bertin & Lin (1996). Rather, it supports the general picture of spiral structure generation that I have been advocating (*e.g.* Sellwood & Lin 1989; Sellwood 2000).

Since a spiral pattern should extend outwards from an ILR, it is somewhat surprising to find evidence for one this far out in the Galaxy. However, the transient spiral waves manifested by simulations of disc galaxies have a wide spread of pattern speeds (*e.g.* Sellwood 1989), and do generally include some spirals in the far outer parts of the disc. The actual pattern speed implied by this resonance and the radii of corotation assuming it is a 2-, 3- or 4-armed spiral, are given in Table 1; the value for $m = 2$ is clearly lower than other estimates for spirals in the Milky Way (see Gerhard 2010, for an up-to-date summary). While the many assumptions, such as the slope of the local rotation curve, the value of the LSR, the neglect of non-axial symmetry, *etc.*, are potential sources of large systematic errors in the *values* given in Table 1, I have argued that none compromise the existence of the resonance. If the disturbance responsible for the ILR is a spiral, then a multi-arm pattern seems more likely than a bi-symmetric one, but it may also have resulted from some other type of slowly-rotating disturbance in the outer galaxy, such as a rotating bi-symmetric distortion of the halo.

Once the still more precise and much more extensive data from *Gaia* (Perryman *et al.* 2001) become available, it will be possible to repeat this analysis with far larger samples of stars, and even at locations other than the solar neighbourhood. In particular, it should be possible to follow the azimuthal variation of stars in the resonance discovered here to determine its angular periodicity. It is to be hoped that other resonant scattering features will be found, and it may be possible to piece together the history of spiral waves in the Milky Way.

ACKNOWLEDGMENTS

I thank Scott Tremaine for suggesting that I examine the distribution of phase angles and Tad Pryor for a number of helpful suggestions on the statistical analysis. This work was supported by grants AST-0507323 from the NSF and NNG05GC29G from NASA.

REFERENCES

Antoja, T., Valenzuela, O., Pichardo, B., Moreno, E., Figueras, F. & Fernández, D. 2009, *ApJL*, **700**, L78
Aumer, M. & Binney, J. J. 2009, *MNRAS*, **397**, 1286

Bensby, T., Oey, M. S., Feltzing, S. & Gustafsson, B. 2007, *ApJL*, **655**, L89
Bertin, G. & Lin, C. C. 1996, *Spiral Structure in Galaxies* (Cambridge: The MIT Press)
Binney, J. J. & Lacey, C. G. 1988, *MNRAS*, **230**, 597
Binney, J. & Tremaine, S. 2008, *Galactic Dynamics* 2nd Ed. (Princeton: Princeton University Press), (BT08)
Bovy, J. & Hogg, D. W. 2009, arXiv:0912.3262
Bovy, J., Hogg, D. W. & Roweis, S. T. 2009, *ApJ*, **700**, 1794
Carraro, G., Vazquez, R. A., Costa, E., Perren, G. & Mointinho, A. 2010, arXiv:1006.1277
Chakrabarty, D. 2007, *A&A*, **467**, 145
De Gennaro, S., von Hippel, T., Jefferys, W. H., Stein, N., van Dyk, D. & Jeffery, E. 2009, *ApJ*, **696**, 12
Dehnen, W. 1998, *AJ*, **115**, 2384
Dehnen, W. 2000, *AJ*, **119**, 800
Dehnen, W. & Binney, J. J. 1998, *MNRAS*, **298**, 387
De Simone, R. S., Wu, X. & Tremaine, S. 2004, *MNRAS*, **350**, 627
Eggen, O. J. 1996, *AJ*, **112**, 1595
ESA 1997, *The Hipparcos and Tycho Catalogues*, SP 1200
Famaey, B., Jorissen, A., Luri, X., Mayor, M., Udry, S., Dejonghe, H. & Turon, C. 2005, *A&A*, **430**, 165
Famaey, B., Pont, F., Luri, X., Udry, S., Mayor, M. & Jorissen, A. 2007, *A&A*, **461**, 957
Gerhard, O. 2010, arXiv:1003.2489
Hänninen, J. & Flynn, C. 2002, *MNRAS*, **337**, 731
Helmi, A., Navarro, J. F., Nordström, B., Holmberg, J., Abadi, M. G. & Steinmetz, M. 2006, *MNRAS*, **365**, 1309
Høg, E., Fabricius, C., Makarov, V. V., Urban, S., Corbin, T., Wycoff, G., Bastian, U., Schwekendiek, P. & Wicenc, A. 2000, *A&A*, **355**, L27
Holmberg, J., Nordström, B. & Andersen, J. 2007, *A&A*, **475**, 519
Holmberg, J., Nordström, B. & Andersen, J. 2009, *A&A*, **501**, 941
Kalnajs, A. J. 1991, in *Dynamics of Disc Galaxies*, ed. B. Sundelius (Gothenburg: Göteborgs University) p. 323
Lacey, C. G. 1991, in *Dynamics of Disc Galaxies*, ed. B. Sundelius (Gothenburg: Göteborgs University) p. 257
Lynden-Bell, D. & Kalnajs, A. J. 1972, *MNRAS*, **157**, 1
Nordström, B., Mayor, M., Andersen, J., Holmberg, J., Pont, F., Jørgensen, B. R., Olsen, E. H., Udry, S. & Mowlavi, N. 2004, *A&A*, **418**, 989
Perryman, M. A. C., de Boer, K. S., Gilmore, G., Høg, E., Lattanzi, M. G., Lindegren, L., Luri, X., Mignard, F., Pace, O. & de Zeeuw, P. T. 2001, *A&A*, **369**, 339
Quillen, A. C. 2003, *AJ*, **125**, 785
Quillen, A. C. & Minchev, I. 2005, *AJ*, **130**, 576
Reid, I. N., Turner, E. L., Turnbull, M. C., Mountain, M. & Valenti, J. A. 2007, *ApJ*, **665**, 767
Robin, A. C., Crézé, M. & Mohan, V. 1992, *ApJL*, **400**, L25
Schönrich, R., Binney, J. & Dehnen, W. 2010, *MNRAS*, **403**, 829
Sellwood, J. A. 1989, in *Dynamics of Astrophysical Discs*, ed. J. A. Sellwood (Cambridge: Cambridge University Press) p. 155
Sellwood, J. A. 1994, in *Galactic and Solar System Optical Astrometry* ed. L. Morrison (Cambridge: Cambridge Univ. Press) p. 156

- Sellwood, J. A. 2000, in *Astrophysical Dynamics – in Commemoration of F. D. Kahn*, eds. D. Berry, D. Breitschwerdt, A. da Costa & J. E. Dyson, *Ap. Sp. Sci.*, **272**, 31 (astro-ph/9909093)
- Sellwood, J. A. & Binney, J. J. 2002, *MNRAS*, **336**, 785
- Sellwood, J. A. & Lin, D. N. C. 1989, *MNRAS*, **240**, 991
- Silverman, B. W. 1986, *Density Estimation for Statistics and Data Analysis* (Chapman and Hall, New York)
- Toomre, A. & Kalnajs, A. J. 1991, in *Dynamics of Disc Galaxies*, ed. B. Sundelius (Gothenburg: Göteborgs University) p. 341
- van Leeuwen, F. 2007, *A&A*, **474**, 653